Towards robust cellular image classification: theoretical foundations for wide-angle scattering pattern analysis

Patrick M. Pilarski[1,*] and Christopher J. Backhouse[2]

[1]*Department of Computing Science, University of Alberta, Edmonton, Alberta, T6G 2E8, Canada*
[2]*Department of Electrical and Computer Engineering, University of Alberta, Edmonton, Alberta, T6G 2V4, Canada*
**patrick.pilarski@ualberta.ca*

Abstract: Clinical analysis of light scattering from cellular organelle distributions can help identify disease and predict a patient's response to treatment. This work presents a theoretical basis for the identification of important intracellular distributions from scattering patterns even in the presence of optical and structural variability, and examines how the geometry of an organelle distribution affects key properties of wide-angle (two-dimensional) scattering patterns. Specifically, this work demonstrates how organelle arrangement relates to the size and shape of intensity peaks within simulated scattering images, and how this relationship can affect cell identification when using standard image classification methods.

OCIS codes: (100.5010) Pattern recognition; (290.5825) Scattering theory; (100.2960) Image analysis; (070.0070) Fourier optics and signal processing; (170.1530) Cell analysis; (170.3880) Medical and biological imaging.

References and links

1. A. K. Dunn, "Light Scattering Properties of Cells," Ph.D. thesis, University of Texas at Austin (1997).
2. V. P. Maltsev, "Scanning flow cytometry for individual particle analysis," Rev. Sci. Instrum. **71**(1), 243–255 (2000).
3. X.-T. Su, C. Capjack, W. Rozmus, and C. Backhouse, "2D light scattering patterns of mitochondria in single cells," Opt. Express **15**(17), 10562–10575 (2007).
4. P. M. Pilarski, X.-T. Su, D. M. Glerum, and C. J. Backhouse, "Computational analysis of mitochondrial placement and aggregation effects on wide-angle cell scattering patterns," Proc. SPIE **7187**, 71870J (2009), http://dx.doi.org/10.1117/12.809730.
5. S. Sikder, J. M. G. Reyes, C. S. Moon, O. Suwan-apichon, J. H. Elisseeff, and R. S. Chuck, "Noninvasive mitochondrial imaging in live cell culture," Photochem. Photobiol. **81**(6), 1569–1571 (2005).
6. A. M. Villa, and S. M. Doglia, "Mitochondria in tumor cells studied by laser scanning confocal microscopy," J. Biomed. Opt. **9**(2), 385–394 (2004), http://link.aip.org/link/?JBO/9/385/1.
7. D. C. Wallace, "Mitochondrial diseases in man and mouse," Science **283**(5407), 1482–1488 (1999).
8. C. F. Bohren, and D. R. Huffman, *Absorption and scattering of light by small particles* (Wiley, NY, 1998).
9. C. Liu, C. E. Capjack, and W. Rozmus, "3-D simulation of light scattering from biological cells and cell differentiation," J. Biomed. Opt. **10**(1), 014007 (2005).
10. R. M. Rangayyan, *Biomedical Image Analysis* (CRC Press, Boca Raton, 2004).
11. K. W. Gossage, C. M. Smith, E. M. Kanter, L. P. Hariri, A. L. Stone, J. J. Rodriguez, S. K. Williams, and J. K. Barton, "Texture analysis of speckle in optical coherence tomography images of tissue phantoms," Phys. Med. Biol. **51**(6), 1563–1575 (2006).
12. P. M. Pilarski, X.-T. Su, D. M. Glerum, and C. J. Backhouse, "Rapid simulation of wide-angle scattering from mitochondria in single cells," Opt. Express **16**(17), 12819–12834 (2008), http://www.opticsinfobase.org/abstract.cfm?URI=oe-16-17-12819.
13. N. Kasai and M. Kakudo, *X-Ray Diffraction by Macromolecules* (Springer, New York, 2005).
14. J. L. McClain, Jr., and D. A. Gregory, "Fourier transforms of phase objects and implications for optical correlators," Microw. Opt. Technol. Lett. **25**(6), 406–412 (2000).

#133970 - $15.00 USD Received 25 Aug 2010; revised 13 Oct 2010; accepted 22 Oct 2010; published 26 Oct 2010

1. Introduction

Studies have shown that important structural information is contained within measurements of angular light scattering intensity from a single cell, including the size, shape, and distribution of cellular micro- and nano-structures [1–3]. Emerging wide-angle cytometers can now capture rich two-dimensional (2D) scattering signatures that provide additional insight into the arrangement and makeup of intracellular components [3,4]. This data has great clinical relevance; for example, information about the distribution of mitochondria (metabolically related organelles) within a cell can help predict a number of disorders, including tumor development and the chemotherapy response of breast and lung cancer patients [5–7]. New image analysis and pattern recognition methods to robustly identify and characterize wide-angle cellular light scattering patterns from cells could therefore play an important role in the identification and treatment of disease.

Unfortunately, given the information-rich 2D structure of wide-angle scattering patterns, their interpretation and comparison is challenging. Scattering image analysis and comparison is further confounded by the observation that similar scattering bodies may generate different 2D scattering signatures due to slight rotations, shifts in their optical properties, and/or changes to the exact placement of their internal components [8,9]. The exact intensity at any given point in two scattering signatures (from nearly identical scatterers) can be significantly different. This is especially noticeable at large scattering angles—*i.e.*, the side-scatter domain—where small organelle scattering is the primary source of detected intensity [1,2]. Given this type of variability, image analysis methods that perform a direct comparison between scattering images may not be robust to normal levels of experimental variation, and finding suitable analysis techniques with both predictive power and suitable invariance is a challenging problem.

This image comparison problem is not unique to light scattering. Chronic variability between two instances of the same, or a similar, biological model (*e.g.*, two mammograms captured at different times or angles) is one of the reasons texture-based image analysis metrics—those that examine high-level image characteristics such as the spatial variation and consistency of image intensity—are employed in many biomedical analysis systems, as opposed to direct pixel-by-pixel image comparison [10]. Texture metrics have been used to successfully relate and compare samples even in the presence of experimental noise and/or using data from different patients [10]. In previous work, we demonstrated that these methods facilitate the interrogation of cells based on their simulated 2D light scattering signature [4]. However, there are still questions surrounding the detection ability of texture-based techniques in this setting—*e.g.*, what types of optical changes they can and cannot distinguish.

In this article, we use optical simulation to examine how texture-based scattering image analysis methods function in situations where the arrangement of scatterers (and thus the phase of detected light) may vary between similar samples drawn from medically relevant cell distributions. We then present a discussion of underlying optical constraints that govern the robust interpretation of 2D cellular scattering patterns, and examine how these constraints affect pattern analysis methods and the diagnostic potential of wide-angle cytometry systems. The result is an important observation about the effects of organelle distribution shape and size on key properties of cellular scattering patterns.

1.1. Background on biomedical texture analysis

A number of image analysis methods have been proposed and successfully applied to biomedical image analysis problems [10]. Of note, texture analysis methods have been used in complex medical classification tasks where it is hard to define shape and semantic structure within an image [10]. As described by Rangayyan, texture descriptors quantify a wide range of statistical, local, and regional image characteristics [10]; they include statistical measures based on global intensity information (variance, skewness, kurtosis), spatial co-occurrence techniques that use local image intensity information (Haralick texture measures), and kernel filters that capture regional image information such as the magnitude of edge, ripple, wave,

#133970 - $15.00 USD Received 25 Aug 2010; revised 13 Oct 2010; accepted 22 Oct 2010; published 26 Oct 2010

and spot content (Laws' texture energy measures) [4,10]. When taken together, texture-based descriptors can provide a unique "fingerprint" for each image, characterizing intensity peak breadth, shape, arrangement, and size, as well as general properties like image contrast, entropy, and homogeneity. Our previous work showed that subsets of these texture metrics are useful in classifying simulated wide-angle scattering patterns [4], and work by Gossage *et al.* demonstrated the use of a vector of Haralick and Fourier texture features for classifying phantom tissue distributions from optical coherence tomography (OCT) speckle images [11].

2. Methods for examining the effect of optical changes on scattering signatures

Optical simulation is an important tool for understanding scattering relationships, and several techniques are available to simulate the scattering of light through single cells—*e.g.*, Mie theory [1,8], Finite Difference Time Domain (FDTD) simulation [1,3,9], and Rayleigh-Gans theory [8]. Each method is governed by different computational and physical constraints [3]. In recent work, we presented a computationally inexpensive simulation method—the mtPatterns algorithm [12]—to generate realistic two-dimensional (2D) scattering signatures for organelle populations within a single cell. The mtPatterns algorithm simulates the light scattering of small organelles like the mitochondria using an adaptation of classical X-ray diffraction and Rayleigh-Gans theory. In it, amplitude contributions from a 3D population of coherently irradiated isotropic or anisotropic scattering centers are superimposed onto a 2D receptive plane in the far field. We found that the intensity patterns generated by this method were in agreement with published experimental and simulated (FDTD) results [12].

To examine the effect of phase shifts and optical changes on the analysis of wide-angle scattering patterns, we used the mtPatterns algorithm to simulate images for two simple and contrasting optical situations: *normal (non-shifted) scattering*, Eq. (1), where the far-field amplitude $A(\mathbf{s}')$ at receptive field point $\mathbf{s}'$ is calculated based on the actual path length $|\mathbf{s}'-\mathbf{r}_n|+d^o{}_n$ from a light source to a scatterer (n) to the receptive field, where $\mathbf{r}_n$ is the position of scatterer n and $d^o{}_n$ is the distance from $\mathbf{r}_n$ to the light source; and *phase-shifted scattering*, Eq. (2), where the path length is non-uniformly shifted such that light leaves all organelles with exactly the same phase value (*i.e.*, $d^o{}_n = 0$).

$$A(\mathbf{s}') = \sum_{n=1}^{N} \{\cos[2\pi\cdot(|\mathbf{s}'-\mathbf{r}_n|+d^o{}_n)] - i\sin[2\pi\cdot(|\mathbf{s}'-\mathbf{r}_n|+d^o{}_n)]\} \quad (1)$$

$$A(\mathbf{s}') = \sum_{n=1}^{N} \{\cos[2\pi\cdot(|\mathbf{s}'-\mathbf{r}_n|+0)] - i\sin[2\pi\cdot(|\mathbf{s}'-\mathbf{r}_n|+0)]\} \quad (2)$$

It should be noted that Eq. (1) is the real-space equivalent of Kasai and Kakudo's reciprocal-space scattering amplitude calculation—Eq. (2.11) in Kasai and Kakudo, 2005 [13]—and can be shown to have the same amplitude behaviour as the reciprocal-space equation at any point in the far field.

Using the mtPatterns algorithm and these two amplitude scenarios, we generated a data set of simulated scattering signatures for three medically relevant organelle distribution types: *diffuse*, *peripheral*, and *perinuclear* [4]. These correspond to conditions where the mitochondria of a cell are evenly distributed throughout the cytoplasm (*diffuse*), clustered around the outer membrane of the cell (*peripheral*) or grouped close to the cell nucleus (*perinuclear*). Discriminating between these three aggregation patterns can help identify drug resistance and malignancy in cells [4]. (More detail on these mitochondrial distributions and their clinical relevance can be found in Pilarski *et al.* [4].)

Each simulated cell had an inner and outer radius of $4\mu m$ and $8\mu m$ respectively, and contained either 83, 250, or 677 isotropically scattering organelles of effective radius $0.375\mu m$. As in Rayleigh-Gans simulation, this work assumed that the refractive index difference between scatterers and the surrounding medium was small [8].

#133970 - $15.00 USD Received 25 Aug 2010; revised 13 Oct 2010; accepted 22 Oct 2010; published 26 Oct 2010

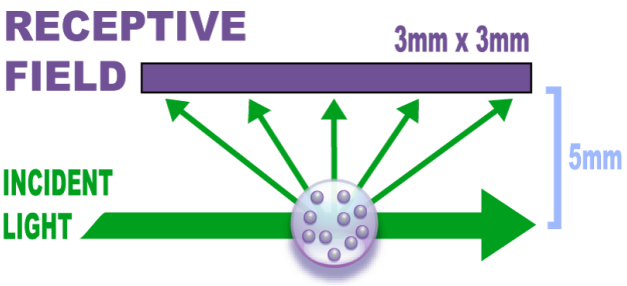

Fig. 1. Schematic diagram of the geometry used in scattering amplitude calculation. The organelle scattering distribution is located 5*mm* below a 3*mm* x 3*mm* receptive field, which runs parallel to the direction of the incident light.

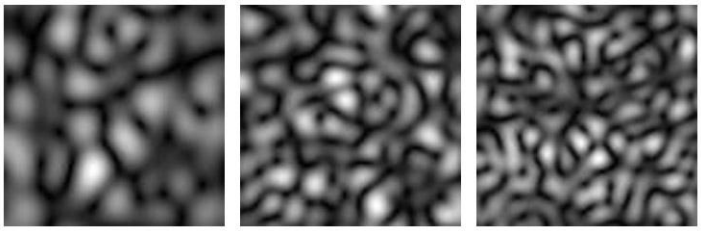

Fig. 2. Example scattering simulations for perinuclear (A), diffuse (B), and peripheral (C) distributions, each made up of 250 organelles and simulated using non-shifted amplitude calculation, Eq. (1). As the size and shape of the distribution changes, so does the size and shape of the intensity regions within its scattering image [4,12].

The cell center was oriented 5*mm* below a 3*mm* by 3*mm* planar receptive field; incident light arrived at the cell parallel to the receptive plane with a wavelength of 632*nm*. This gives an angular observation range of 77.3°–106.7° along both axes of the receptive field. A schematic of this arrangement is shown in Fig. 1; all scattering simulations presented in this work share the same experimental setup and angular range.

Fifteen unique cells were generated for each of the three distribution models, with five cells for each of the three organelle concentration levels; organelles were arranged randomly within each distribution. Shifted and non-shifted scattering patterns were then simulated for each cell, giving a total of 45 labeled images for Eq. (1) and 45 labeled images for Eq. (2). Examples of these images appear in Fig. 2. Simulated images were then compared using twenty-one of the standard texture analysis measures introduced in Sec. 1.1: skewness, kurtosis, variance, eleven Haralick features (H1–H11), and seven Laws' texture energy measures (E5, S5, S5x2, S5x4, W5, R5, L5) [4,10]. These algorithms were implemented as per Rangayyan 2004 [10]. Each of these texture features presents a different aspect of scattering image structure—for example, Laws' spot content relates to the quantity of intensity peaks of a given size in an image, while features like Laws' edge content and Haralick local homogeneity relate to peak width. For the purpose of analysis, the set of texture measures for each image was represented as a twenty-one-item feature vector. Given that the magnitude and possible range of texture feature values varies across metrics, in what follows we discuss the difference between images in terms of the number of statistically significant element-by-element differences between two feature vectors, using the within-class standard deviation from the full data set. This difference is in effect the hamming distance between two images or image populations in terms of their "fingerprint" or collection of texture analysis measures.

#133970 - $15.00 USD Received 25 Aug 2010; revised 13 Oct 2010; accepted 22 Oct 2010; published 26 Oct 2010

3. Analysis of simulated scattering images

Comparison of the shifted and non-shifted methods for amplitude calculation across cell models presented an interesting result: while a direct pixel-by-pixel comparison of resulting scattering images showed the expected differences between shifted and non-shifted patterns, the effect of the non-uniform phase shift was largely invisible to a number of standard image processing metrics used for biomedical data analysis and comparison [4,10]. These texture-based validation and processing methods—e.g., methods that characterize intensity region size, spacing, orientation, and shape—were sensitive to medically relevant changes in intracellular structure [*i.e.*, organelle distribution), but robust to random organelle shifts and noise (such as the non-uniform shift in phase present in Eq. (2)].

To characterize this difference between shifted and non-shifted simulation results, we note that the modified path difference in Eq. (2) introduces an additional phase shift $\tau(\mathbf{r}_n)$ that is dependent on the exact position of each scatterer. When written in terms of a Fourier transform, scattering in the shifted case can be represented as shown in Eq. (3):

$$A(\mathbf{S}) = \mathcal{F}\{\rho(\mathbf{r}_n) exp[2\pi i \mathbf{S}\cdot\tau(\mathbf{r}_n)]\}, \tag{3}$$

where $\rho(\mathbf{r}_n)$ defines the scatterer placement and $\tau(\mathbf{r}_n)$ is a phase shift from $(-\pi, \pi]$ that is a function of the distance between a scattering point $\mathbf{r}_n$ and the light source or reference plane. For all but the simplest cases, it is extremely difficult (or impossible) to find an analytical solution to the Fourier transform of non-uniform phase shifts [14]. However, more general relationships have been identified. As shown by McClain and Gregory, a *phase-only shift* to points in the scatterer distribution relates to a corresponding *positional shift* to intensity peaks in the Fourier (scattering) plane [14]. An example of this can be seen experimentally in Fig. 3—while the location of intensity peaks in the image changes between the phase-shifted and non-phase-shifted populations, average peak breadth and spacing appear to remain relatively static. Comparing the feature vectors from the non-shifted and shifted simulation images in Fig. 3(C) and 3(D), we found that the difference between paired values was significantly smaller than the within-group standard deviation for seventeen of the twenty-one texture feature pairs. The difference for the remaining four pairs was only slightly higher than one standard deviation, and still well below the observed between-group separation. Despite the varied arrangement of intensity regions in the two images, we found no major differences between the images in terms of image texture.

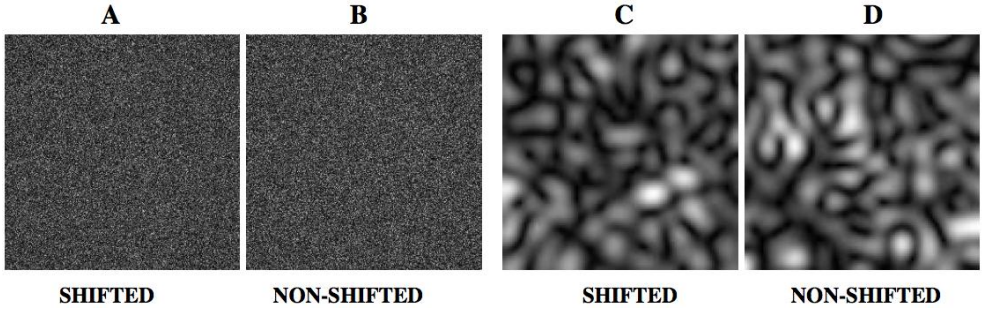

Fig. 3. LEFT: The effect of a phase perturbation on a population's simulated scattering pattern, using a very wide distribution aperture (minimal shape effects): scattering using shifted phase values (A), and scattering using non-shifted phase values (B) for 1000 scatterers, placed randomly in a 1500μm radius sphere. RIGHT: Comparison of the simulated wide-angle scattering patterns for a mitochondrial distribution simulated by the mtPatterns algorithm, using the shifted equation (C) and non-shifted equation (D) for 300 scatterers, placed randomly in a diffuse cellular distribution with an inner and outer radius of 4μm and 8μm respectively. In both cases, average peak breadth does not change noticeably due to phase perturbation.

#133970 - $15.00 USD Received 25 Aug 2010; revised 13 Oct 2010; accepted 22 Oct 2010; published 26 Oct 2010

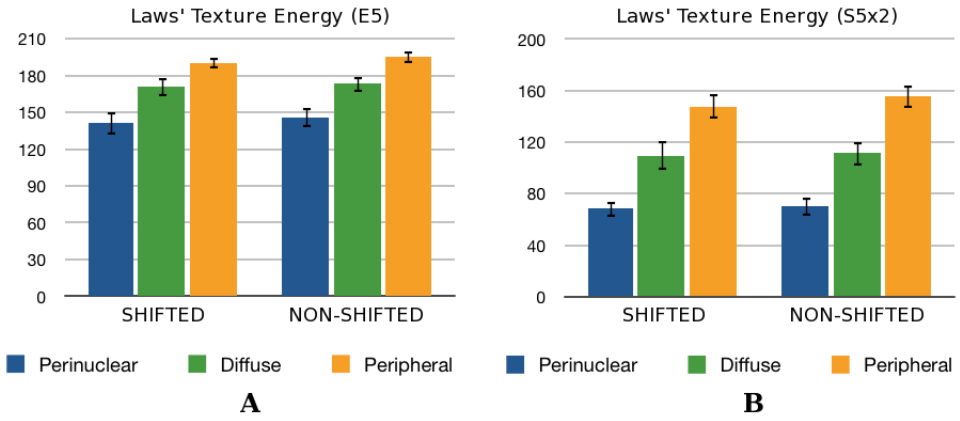

Fig. 4. Comparison of simulated scattering pattern data sets in terms of standard image descriptors representing the edge (A) and spot (B) content in scattering images. Edge content is represented by the Laws' Texture Energy E5 kernel (E5) while spot content is represented by the Laws' Texture Energy S5 kernel, scaled by a factor of two (S5x2). Tests were performed for three different distribution types, with fifteen samples per distribution, per trial. As shown here, the difference between texture values for different organelle distribution classes was much greater than the difference observed between the non-shifted and shifted patterns.

Next we compared the difference between feature vectors for the full data set of non-shifted and shifted simulation images from the perinuclear, diffuse, and peripheral distribution models, averaged over all fifteen images (cell models) for each distribution class. We found that the texture similarity observed for the two images in Fig. 3 extended to the full data set—while the exact position of intensity peaks within scattering patterns changed as a result of an arbitrary phase shift or organelle population perturbation, the corresponding feature vectors did not change in a significant way. In other words, the average breadth, spacing, and shape of intensity peaks remained constant despite a random repositioning of organelles or the phase shift from Eq. (2). An example of this is shown in Fig. 4, for two of the texture measures used in this study: Laws' Texture Energy E5 (Fig. 4, left), and Laws' Texture Energy S5x2 (Fig. 4, right). These features represent the levels of edge and spot content in an image, as sampled by the Laws' E5 kernel and scaled S5 kernel respectively [10]. As shown in Fig. 4, for these two measures the difference between the average texture value for non-shifted and shifted scattering image populations was not statistically significant. The behaviour observed in Fig. 4 is representative of the majority of the other texture measures.

To illustrate this, Fig. 5 presents a more detailed comparison of the texture differences between the shifted and non-shifted cases for all twenty-one texture features. This comparison is done in terms of the ratio of the within-group (*i.e.*, distribution class) standard deviation to the average separation between groups [Fig. 5(a)], and the ratio of the difference between shifted/non-shifted cases to the average between-group separation and to the average within-group standard deviation [Fig. 5(b)]. In all cases the difference between texture values for different organelle distribution classes was much greater than the difference observed between the non-shifted and shifted patterns [Fig. 5(b), blue; all ratios were significantly below unity]. The mean difference between non-shifted and shifted patterns was also consistently smaller than the within-group standard deviation [Fig. 5(b), yellow]. As shown in Fig. 5(a), Laws' Texture Energy Measures maintained the smallest within-group standard deviation when compared to the feature value differences between distribution types, along with statistical skewness and Haralick features for image homogeneity (H1) and image entropy (H8, H9, H11). This is consistent with prior results suggesting that Laws' features may be a good basis for scattering pattern classification [4], and the success of entropy and homogeneity features in tissue phantom OCT studies [11].

#133970 - $15.00 USD Received 25 Aug 2010; revised 13 Oct 2010; accepted 22 Oct 2010; published 26 Oct 2010

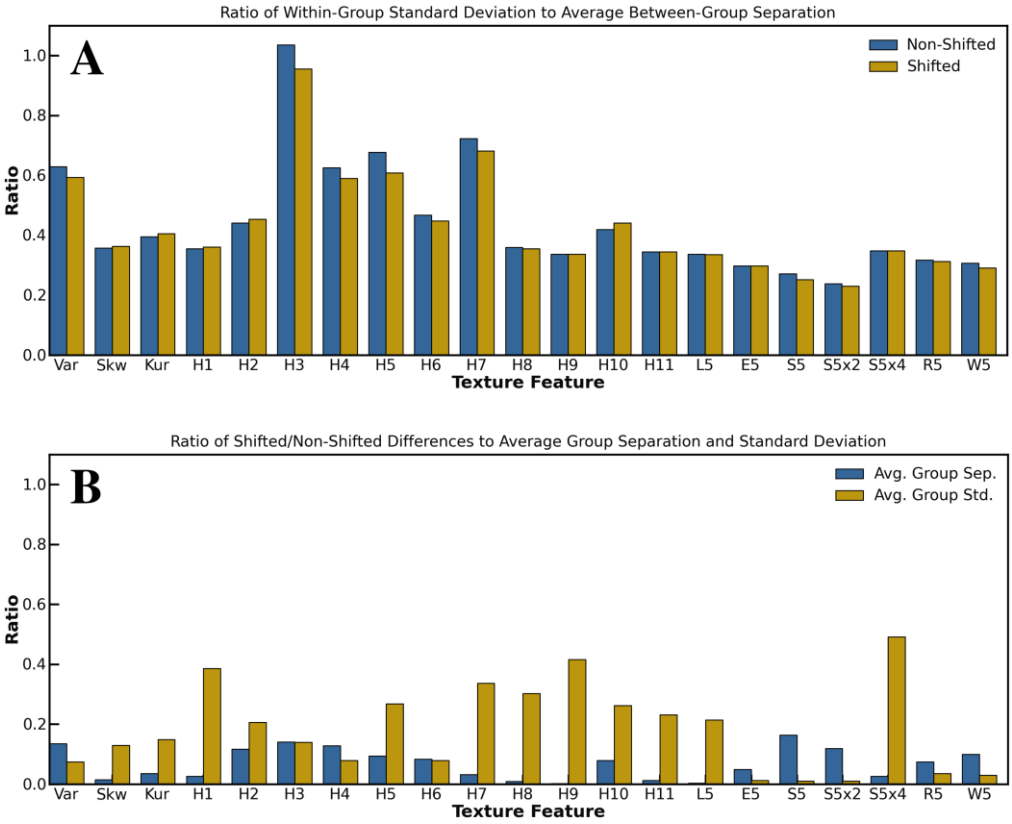

Fig. 5. Comparison of shifted/non-shifted image differences in terms of twenty-one texture features, specifically: (A) the ratio of the within-group (*i.e.*, distribution class) standard deviation to the average separation between groups, and (B) the ratio of the difference between shifted/non-shifted cases to the average between-group separation and to the average within-group standard deviation.

4. Discussion of robust behaviour and its impact on image analysis methods

As demonstrated in Figs. 3–5, changing between non-shifted and shifted scattering calculation methods—Eq. (1) and Eq. (2) respectively—had no major effect on key qualitative aspects of simulated wide-angle organelle scattering patterns. The texture-based features studied in this work remained invariant to small optical and structural changes within a distribution. This was confirmed on the full data set of simulated scattering images from differing distribution classes and organelle concentrations. At the same time, the studied texture features were good indicators for the class of organelle distribution responsible for a particular scattering signature. This is observed in the small difference between feature vectors for the two scattering calculation algorithms on any given distribution class, as compared to the difference between feature vectors for different distribution classes [Fig. 4 and Fig. 5(b)].

While at first surprising, these observations agree with expectations from X-ray diffraction theory and Fourier optics. As described by Kasai and Kakudo, when the size of a scattering distribution is relatively small with respect to the spacing between individual scatterers, the breadth and shape of intensity peaks in the scattering plane is dominated by a distribution's *shape factor* (also known as an aperture function)— *i.e.*, the size and shape of the scattering distribution, as opposed to the exact placement of individual scatterers [13]. Conversely, if the spacing between scatterers is much smaller than the size of the distribution (for instance, the case of a very large or infinitely wide crystal), peak breadth is instead determined by the relationship between individual scatterers (for example, their spacing and placement) [13].

#133970 - $15.00 USD Received 25 Aug 2010; revised 13 Oct 2010; accepted 22 Oct 2010; published 26 Oct 2010

This knowledge is used in crystallography to help determine the size and shape of crystals, paracrystals, and amorphous scattering bodies [13]; a detailed treatment is provided in Chapter 13 of Kasai and Kakudo, 2005 [13].

For the case of scattering from organelle populations similar to the mitochondria in a human cell, we have the former case: the spacing between organelles is typically only one to two orders of magnitude less than the width of the cell itself. As such, we expect the breadth and shape of intensity peaks in the scattering pattern to be determined by the distribution's shape factor—*i.e.,* to be "diffraction limited" by the shape and size of the distribution of scatterers, as opposed to the spacing and arrangement of individual scatterers. As phase perturbations in the scatterer domain are known to lead to positional shifts in the Fourier domain (as per McClain and Gregory [14]), we expect their impact on peak size and shape to be negligible compared to the broadening effect from the distribution's shape factor. This is precisely what was observed with the comparison of shifted and non-shifted cases in Sec. 3.

It then follows that image analysis techniques based on texture will be largely unaffected by these changes. Texture measures are based on the size and relationship between intensity regions—things that, for realistically constrained examples of the cellular scattering case, appear to be largely determined by the size and shape of the scattering distribution and not the exact placement or optical alignment of scatterers. This helps explain why the non-uniform phase shift between Eq. (1) and Eq. (2) does not have a noticeable impact on, and may not be detected by, many texture-based processing routines. When paired with these observations from X-ray diffraction theory, the results presented in Sec. 3 also suggest that changes to the number/concentration of scatterers may have minimal impact on peak breadth and shape. The shift in scatterer spacing due to realistic organelle concentration changes should not be large enough to overcome the broadening due to distribution shape. This is consistent with recently published results, where we found that organelle concentration in simulated samples was poorly correlated with scattering peak size and shape [4].

These observations about the robust properties of texture-based features are further supported by results from the OCT literature regarding the classification of tissue type from backscattered speckle images. OCT speckle images are typically sampled over a fixed angular range in the backscattering region, and concern near-infrared light re-radiated or reflected by a population of cells within a tissue sample (as opposed to organelles within a single cell) [11]. While different in terms of scale and optical alignment, speckle analysis shares a number of properties with wide-angle single-cell scattering analysis. Intensity patterns captured by both methods are qualitatively similar, and pattern composition in both scenarios appears to be governed by the high-level properties of a 3D distribution of scattering centers. In particular, it has been shown that while it is difficult or impossible to use speckle patterns to ascertain the exact arrangement of cells in a tissue sample, the texture information present in speckle patterns may provide unique profiles able to classify both tissue type and disease state [11].

As in wide-angle cytometry, image processing methods have shown promising results for speckle analysis. Specifically, recent work by Gossage *et al.* demonstrated accurate tissue phantom classification using a texture feature vector that contained metrics similar those used in the present work (*i.e.*, Haralick features based on a co-occurrence matrix, such as local homogeneity, entropy, energy, correlation, and inertia) [11]. These findings from speckle analysis reinforce the idea that texture features may be a good basis for classifying wide-angle scattering patterns from single cells, and that certain texture features will remain invariant to small shifts in intracellular arrangement or phase. The analogy between speckle analysis and wide-angle cytometry is an interesting area for further study, and the work of Gossage *et al.* indicates that the use of Fourier transform texture features may provide additional classification power in a wide-angle cytometry setting.

The experiments presented in this work dealt with a fixed angular range in the side-scattering region that is known to contain relevant information about microstructural scatterers. While initial experiments have been conducted into using these analysis methods over other angular ranges, this remains an important area for future investigation. Similarly, an extension of this work to more complex cellular scattering situations with varying optical

#133970 - $15.00 USD Received 25 Aug 2010; revised 13 Oct 2010; accepted 22 Oct 2010; published 26 Oct 2010

properties and anisotropy (for instance, using 3D FDTD simulation and wide-angle cytometry trials with labeled human cells) is required to determine the full extent of the texture-related robustness and classification ability suggested by the present study.

5. Conclusions

This work presented a theoretical perspective on the identification of intracellular distributions from wide-angle scattering patterns even in the presence of optical and structural variability. Specifically, it used simulation to demonstrate that the breadth and shape of intensity peaks in wide-angle cellular scattering patterns may be dominated by a scattering distribution's *shape factor* (*i.e.,* a 3D distribution's shape and size), as opposed to broadening due to phase variation or scatterer placement. These observations are important for cellular scattering pattern analysis. It appears that—at least in terms of scattering peak geometry—the shape factor of a scattering distribution will overwhelm changes due to organelle placement and concentration. As such, metrics based on image texture, specifically the shape and size of intensity peaks, seem resilient to the randomness and variability that challenges direct image comparison methods. At the same time, they remain sensitive to structural changes of medical interest—*e.g.,* the distribution of scatterers like the mitochondria.

This points to a robust set of texture-related tools for analyzing and classifying organelle distributions based on wide-angle (2D) cellular scattering patterns. However, it also indicates that it may be difficult or impossible to determine exact scatterer position and concentration from a wide-angle scattering signature using only the shape, size, and spacing of intensity peaks. This is an interesting avenue for further study.

While the results in this work are consistent with expectations from Fourier scattering theory and our preliminary analysis of real-world cytometry data, additional experimental results are needed to confirm whether the conclusions drawn from this idealized simulation domain hold for the wide-angle scattering signatures from complex, heterogeneous human cells. Future work will address this question, and explore methods to determine both distribution shape and scatterer concentration from a single scattering image.

Acknowledgements

This work was made possible by financial support from the Natural Sciences and Engineering Research Council (NSERC) and the Canadian Institute for Photonic Innovations (CIPI). PMP was supported by NSERC, SPIE, Alberta Ingenuity, and the Informatics Circle of Research Excellence (iCORE).

#133970 - $15.00 USD Received 25 Aug 2010; revised 13 Oct 2010; accepted 22 Oct 2010; published 26 Oct 2010